



# A variational model for dynamic recrystallization based on Cosserat plasticity

T. Blesgen

Bingen University of Applied Sciences, Berlinstraße 109, D-55411 Bingen, Germany

## ARTICLE INFO

### Article history:

Received 26 July 2016

Received in revised form 29 September 2016

Accepted 2 October 2016

Available online xxx

### Keywords:

Dynamic recrystallization

Plasticity

Cosserat theory

Softening

## ABSTRACT

A hardening model within the framework of finite-strain Cosserat crystal plasticity is extended to dynamic recrystallization. The new model includes an Avrami equation to account for softening, a level set equation to represent the propagation of the domain walls, and the Ambrosio-Tortorelli approach inherited from image analysis to identify the grain dislocation structure. Numerically, flow curves are computed and the Hall-Petch relation is studied.

© 2016 Published by Elsevier Ltd.

## 1. Introduction

During plastic deformation dislocations are generated, moved, and finally stored in a crystal which makes itself felt as work hardening. At low temperatures the dislocation structure is thermodynamically unstable but mechanically stable, and thus does not change with time. If the temperature is raised, diffusion mechanisms are activated and the crystal can lower its free energy by removing dislocations either by annihilation and/or rearrangement or by the nucleation of strain-free grains which expand at the expense of the deformed structure. The former process is referred to as recovery, the latter is termed recrystallization. If deformation occurs during elevated temperatures, i.e. hot working, recrystallization is liable to occur during deformation. This is called dynamic recrystallization (DRX), in contrast to static recrystallization (SRX) which occurs slowly due to diffusion processes after the deformation.

During hot working of steels or alloys DRX is a common phenomenon. Despite its industrial importance and extensive research in the field, recrystallization and, in particular, DRX, are still not comprehensively solved problems of physical metallurgy. The present paper aims at developing a model that is capable to capture the essential phenomena of dynamic recrystallization and to provide predictions of microstructure development and mechanical behavior of materials during hot working.

There have been many attempts in the past to address DRX. In Ref. [26], a simple model was introduced where DRX is considered as a superposition of deformation and static recrystallization on the basis of Avrami kinetics. This allows to fit measured flow curves and to explain the occurrence of single and multiple peak flow curves. However, the controlling quantities like a critical strain have to be derived from the measured flow curves [37]. Associates the occurrence of sin-

gle and multiple peak flow stress behavior with the tendency to grain refinement and grain coarsening during DRX, but struggles to explain why the transition occurred at twice the steady state grain size. A quite different approach was proposed in [32] on the basis of irreversible thermodynamics. Therein, the critical strain is defined by the condition of minimum energy dissipation at maximum energy storage. Using the one-parameter model of Hart [19], for work hardening, it was shown in [32] that this point coincides with the point of inflection on the so-called “Kocks-Mecking-plot”, where the strain hardening rate is plotted versus the flow stress, [28]. In fact, the evaluation of experimental results shows that the beginning of DRX occurs close to this point, although a point of inflection can also occur without DRX, e.g., during high temperature deformation of high stacking fault energy materials like aluminum, where a steady state flow stress is obtained by equilibrium between dynamic recovery and work hardening. There are many more modeling studies on DRX in literature, but most of them are based on empirical relations since monotonic dependencies can – at least piecewise – be approximated by power laws. In Refs. [13] [34], the dynamically recrystallized grain size was addressed particularly by making assumptions on the relevant criteria like back stresses at grain boundaries or imbalance of subgrain size across prior grain boundaries, but the issue of mechanical behavior was not touched.

Evidently, despite extensive research during the past decades, the physical mechanisms of dynamic recrystallization are not yet satisfactorily understood. The subject is not only of academic interest but is also of immense importance for industrial processing, e.g. hot rolling: dynamic recrystallization offers a powerful tool for microstructure control and, therefore, a useful way for the optimization of the sheet properties, [21,33,43].

A numerical study of DRX in two dimensions is available in [17]. The ansatz is based on a level set approach and a rate-equation for the nucleation of new grains. The treatment of plasticity is simplified and

Email address: t.blesgen@th-bingen.de (T. Blesgen)

the macroscopic plastic strain is assumed to follow the Kocks-Mecking relation.

In [15], based on homogenization techniques, see [44] for a review, the influence of the grain structure on the mechanical properties is studied. In [3], the viscoplastic case is treated with the help of higher-order gradients in the hardening law. Surveys of DRX models are available in Refs. [35,27].

In this article, a variational model is developed which builds on the finite-strain Cosserat theory of crystal plasticity. It incorporates the multiple facets of DRX and is thus rather elaborate. The proposed model extends the analytical and numerical studies in Refs. [8–10]. In [7], the coupling of plasticity and phase transitions for simpler systems had been investigated.

This article is organized in the following way. In Section 2, the physical model is derived. Section 3 outlines details of the numerical implementation. Section 4 is devoted to simulations. The article ends with a discussion.

## 2. The physical model of dynamic recrystallization

For simplicity, the temperature  $T$  is assumed constant. The model developed subsequently consists of two main parts. The first part, formulated within the Cosserat theory of crystal plasticity, is governed by minimization of the mechanical energy, cf. Section 2.2. For simplicity, individual dislocations are not resolved, but instead a function  $\kappa \leq 0$  is introduced, the (scalar) hardening parameter of the material. The mechanical energy of the stored immobile dislocations is represented by a potential  $V$  without resolving the local distribution of mobile, geometrically necessary and locked dislocations in the solid.

The second part of the model is concerned with softening. It cannot be formulated by energy minimization as will be explained later. This part includes recovery due to climbing dislocations as well as the formation of new grains essentially free of dislocations. This requires the (automated) identification and computation of the grain structure, as outlined in Section 2.1. New grains are nucleated if critical conditions are reached, cf. Section 2.4.

Subsequently the main aspects of dynamic recrystallization are collected. The complete model is summarized in Section 2.5.

### 2.1. Grain orientation and partitioning into subgrains

The simulated material is a polycrystal. As is well known, see e.g. [16], the grains of a polycrystal are separated by regions occupying a small volume containing the geometrically necessary dislocations as well as redundant dislocations. Fundamentally, it is assumed that neighboring grains differ in their local orientation so that by knowing the vector of micro-rotations  $\alpha^0 \in (H^1(\Omega; [0, 2\pi]))^3$ , a parameterization by Euler angles, the complete (sub-)grain structure in the entire crystal can be determined. Here,  $H^m(\Omega) \subset L^2(\Omega)$  denotes the Sobolev space of  $m$ -times weakly differentiable square-integrable functions in  $\Omega \subset \mathbb{R}^3$ , the reference state of the material. For known  $\alpha^0 = (\alpha_1^0, \alpha_2^0, \alpha_3^0)$ , the local orientation of the (sub)-grains at a spatial point  $x \in \Omega$  is specified by

$$R(\alpha^0(x)) \in \text{SO}(3) := \{Q \in \text{GL}(3) \mid \det(Q) = 1, Q^t Q = \text{Id}\},$$

with the mapping  $R: [0, 2\pi)$  given by (cf [10])

$$R(\alpha) := \begin{pmatrix} 1 & 0 & 0 \\ 0 & \cos \alpha_3 & \sin \alpha_3 \\ 0 & -\sin \alpha_3 & \cos \alpha_3 \end{pmatrix} \begin{pmatrix} \cos \alpha_2 & 0 & -\sin \alpha_2 \\ 0 & 1 & 0 \\ \sin \alpha_2 & 0 & \cos \alpha_2 \end{pmatrix} \begin{pmatrix} \cos \alpha_1 & \sin \alpha_1 \\ -\sin \alpha_1 & \cos \alpha_1 \\ 0 & 0 \end{pmatrix}$$

For the first time step,  $g(x) := (g_1, g_2, g_3)(x) \in BV(\Omega; [0, 2\pi])^3 \cap L^\infty(\Omega)$  are the measured Euler angles, taken from Electron Backscatter Diffraction (EBSD) experiments. Here,  $BV(\Omega)$  is the space of functions of bounded variation and  $L^\infty(\Omega)$  the essentially bounded functions in  $\Omega$ . The input data  $g$  is converted into a smoothed field  $\alpha^0$  which tends to be piecewise constant as follows. Following [5] where the Mumford-Shah functional from image analysis is approximated by elliptic functionals, for  $l \in \{1, 2, 3\}$ , constants  $\sigma > 0$ ,  $\tau > 0$ , and with  $H^d$  denoting the  $d$ -dimensional Hausdorff measure, the functional

$$G(\alpha_l^0, D_l) := \int_{\Omega \setminus D_l} \left[ \tau (\alpha_l^0 - g_l)^2 + |\nabla \alpha_l^0|^2 \right] dx + \sigma \mathcal{H}^2(D_l) \quad (2)$$

is considered. The first integrand in (2) ensures that  $\alpha_l^0 \in H^1(\Omega \setminus D_l)$  approximates the given  $g_l$ . The second term  $|\nabla \alpha_l^0|^2$  favors constant  $\alpha_l^0$ . When minimizing  $G$ ,  $D_l \subset \Omega$  approaches the discontinuities of  $g_l$ , i.e. the optimal  $D_l$  is the (closed) jump set of  $\alpha_l^0$ .

Instead of optimizing sets, it is more convenient to optimize functions. In the spirit of [5], by applying methods from  $\Gamma$ -convergence, it can be shown that  $G$  for small  $\delta > 0$  can be approximated by

$$G_\delta(\alpha_l^0, v_l) := \int_{\Omega} \left[ (|\nabla \alpha_l^0|^2 + |\nabla v_l|^2) (1 - v_l^2)^{2/\delta} + \frac{\sigma^2}{4\delta^2} v_l^2 \right] dx + \tau \int_{\Omega} dx$$

Here,  $v_l \in [0, 1]$  is a control variable on  $\nabla \alpha_l^0$ , representing the geometrically necessary dislocations in the material. In the limit  $\delta \searrow 0$ ,  $\text{supp}(\nabla v_l)$  converges to the set of discontinuities of  $\alpha_l^0$ , i.e. to a minimizer  $D_l$  of  $G$ .

Eqn. (3) is related to the ansatz in Refs. [1,2]. Therein, a two-dimensional phase-field model for DRX is proposed with a scalar angle parameter (analogous to  $\alpha$ ) and a crystallinity  $\theta$  (analogous to  $v_l$ ). The model in Refs. [1,2] is capable of reproducing many features of DRX, but is only two-dimensional and ignores sub-grain effects. In (3),  $\sigma$  can be interpreted as an (isotropic) surface energy, while  $\delta$ ,  $\tau$  are numerical parameters.

After the minimization of  $G$ , the actual grain partitioning is achieved by a least squares algorithm. Given a constant  $\delta_{\text{TOL}} > 0$ , two points  $x_1, x_2 \in \Omega$  are identified to belong to the same grain, if

$$|\alpha^0(x_1) - \alpha^0(x_2)| < \delta_{\text{TOL}}. \quad (4)$$

Noteworthy, the result of this identification process is independent of the order by which the points  $x_i \in \Omega$  are picked, since the minimizers  $\alpha^0$  of  $G_\delta$  are piecewise constant.

## 2.2. Plasticity and hardening

The plastic behavior of the solid is modeled within the framework of the large-strain Cosserat theory of crystal-plasticity. Up to certain modifications, the ansatz from Refs. [8,9] is re-used. As a fundamental assumption, it is postulated that if the mechanical properties at time  $t=nh$  are known, where  $h>0$  is a fixed time step and  $n \in \mathbb{N}$ , the state of the solid at time  $t=(n+1)h$  can be obtained by minimizing the total mechanical energy  $E$  in suitable spaces, cf. Eqn. (7) below.

Let  $\Omega_t = \varphi(\Omega, t)$  for a family of diffeomorphisms  $\varphi(\cdot, t)$  in  $\mathbb{R}^3$  be the deformed polycrystal at time  $t$ . At the heart of the Cosserat approach, the deformation tensor  $F := D\varphi$  is multiplicatively decomposed,

$$F = F_e F_p = R_e U_e F_p, \quad (5)$$

with  $F_e, F_p$  denoting the elastic and plastic deformation tensors,  $U_e \in \text{GL}(3)$  the stretching component, and  $R_e \in \text{SO}(3)$  the micro-rotations. In Eqn. (5),  $U_e$  need not be symmetric and positive definite, i.e. the decomposition  $F_e = R_e U_e$  is *not* the polar decomposition. As in (1),  $R_e = R_e(\alpha) \in \text{SO}(3)$  is parameterized non-uniquely by a vector of Euler angles  $\alpha = (\alpha_1, \alpha_2, \alpha_3)$ .

The plastic deformations are assumed to occur along  $I_p \geq 1$  a-priori given material-dependent single-slip systems, only. These slip systems are specified by tensors  $m_a \otimes n_a$ , where  $m_a$  denotes the slip vector and  $n_a$  the slip normal of slip system  $a$  for  $1 \leq a \leq I_p$ . These vectors satisfy  $|m_a| = |n_a| = 1$  and  $m_a \cdot n_a = 0$ . For  $\gamma = (\gamma_a)_{1 \leq a \leq I_p} \in \mathbb{R}^{I_p}$ , it is thus set

$$F_p = F_p(\gamma) := \text{Id} + \sum_{a=1}^{I_p} \gamma_a m_a \otimes n_a. \quad (6)$$

As a result of plastic deformation, due to structural changes within the material like the increase of immobilized dislocations, hardening occurs, see e.g. Refs. [12,7]. In the model,  $\kappa$  is a (non-positive) scalar hardening parameter, with  $-\kappa \geq 0$  representing the density of immobilized dislocations. In the model,  $\kappa$  also depends on a recovery parameter  $\kappa^r$ . This is why the derivation of a formula for  $\kappa$  is postponed to Section 2.3.

To conclude, for vectors  $\alpha^0, \gamma^0$  representing data of the previous time step, the evolution of a plastically deformed solid in the absence of surface tractions and surface couples in the Cosserat theory of rate-independent large-strain crystal-plasticity is governed by the time-discrete minimization problem

$$\mathcal{E}(\varphi, \alpha, \gamma, \kappa^r) := \int_{\Omega} \left[ W_{\text{st}}(R_e^t(\alpha) D\varphi F_p(\gamma)^{-1}) + 2\mu_2 \left| \nabla \alpha \right|_2^2 - f_{\text{ext}} \cdot \varphi - V(\kappa(\gamma, \kappa^r)) + \mu_3 \left| \alpha - \alpha^0 \right|_2^2 + \sigma_Y \sum_{a=1}^{I_p} \left| \gamma_a - \gamma_a^0 \right| \right] dx \rightarrow \min$$

subject to the initial and boundary conditions

$$\begin{aligned} \varphi(x, 0) &= x, & \kappa(\cdot, 0) &= \kappa^0 & \text{in } \Omega, \\ \varphi &= \varphi_D & & & \text{on } \partial\Omega. \end{aligned} \quad (8)$$

The choice in (8) corresponds to Dirichlet boundary conditions for  $\varphi$  and free boundary conditions for  $\alpha$ .

In (7),  $f_{\text{ext}}(t), M_{\text{ext}}(t)$  denotes the external volume force densities and the external volume couples applied to the crystal body;  $\sigma_Y > 0$  is the yield stress. Eqn. (7) introduces a family of time-discrete minimization problems. The concept goes back to [14], see also [31], and permits the application of the calculus of variations to plasticity. For the fixed discrete time step  $h > 0$  and known  $(\alpha^0, \gamma^0, \kappa^0)$  at time  $t$ , the new  $(\varphi, \alpha, \gamma, \kappa)$  representing values at time  $t+h$  is calculated from (7). Finally,  $\kappa = \kappa(\gamma, \kappa^r)$  is computed and  $(\alpha, \gamma, \kappa)$  are set as the initial values  $(\alpha^0, \gamma^0, \kappa^0)$  of the next time step.

The term  $\mu_3 \left| \alpha - \alpha^0 \right|_2^2$  with  $\mu_3 > 0$  differs from the formulation in Refs. [8,9] and bounds the variation of  $\alpha$  in time. It is required to link the (micro-)rotations of the Cosserat solution to the measured rotation field.

The definitions of the remaining functionals are taken from Refs. [8,9]. They are repeated here for convenience. Let  $L_c > 0$  be the internal length scale,  $\mu > 0, \lambda > 0$  the Lamé parameters,  $\mu_c \geq 0$  the Cosserat couple modulus, and  $\mu_2 := \frac{\mu}{2} L_c^2$ . For the energy of stored dislocations, the simple quadratic ansatz is made,

$$V(\kappa) := \varrho \kappa^2$$

where  $\varrho > 0$  is a constant. The curvature energy due to (micro) rotations is

$$W_c(\alpha) := 2\mu_2 \left| \nabla \alpha \right|_2^2 := 2\mu_2 \sum_{l=1}^3 \left| \nabla \alpha_l \right|^2 \quad (9)$$

and the stretching part of the mechanical stored energy density is, cf. [30],

$$W_{\text{st}}(U_e) := \mu \left\| \text{sym} U_e - \text{Id} \right\|^2 + \mu_c \left\| \text{skw}(U_e - \text{Id}) \right\|^2 + \frac{\lambda}{2} \text{tr}(U_e - \text{Id})$$

Here,  $\text{sym} A := \frac{1}{2}(A + A^t)$ ,  $\text{skw} A := \frac{1}{2}(A - A^t)$  denote the symmetric and skew-symmetric parts of a tensor  $A$ , respectively,  $\text{tr}(A) := \sum_i A_{ii}$  is the trace operator,  $\|A\| := \text{tr}(A^t A)$  the Frobenius matrix norm. For  $\mathbf{u}, \mathbf{v} \in \mathbb{R}^3$ ,  $\mathbf{u} \cdot \mathbf{v} := \sum_{i=1}^3 u_i v_i$  is the inner product in  $\mathbb{R}^3$ . For tensors  $A, B \in \mathbb{R}^{3 \times 3}$ ,  $A : B := \text{tr}(A^t B) = \sum_{i,j=1}^3 A_{ij} B_{ij}$  denotes the inner product in  $\mathbb{R}^{3 \times 3}$ .

### 2.3. Softening and the formation of new grains

Two mechanisms are responsible for the softening of the alloy. Firstly, climbing dislocations continuously lead to a dynamic recovery of the material. Secondly, on a small length scale, new nuclei essentially free of dislocations are generated perpetually due to thermal ac-

tivation. In the early stages, while its size is below a critical threshold, the growth of such a nucleus is energetically unfavorable as the gain in volume energy cannot compensate the loss of surface energy. (This is the reason why the process is not cast into an energy minimization formulation.) Consequently, a small nucleus can only grow at the expense of other, even smaller nuclei and will eventually disappear in most cases.

In this article, the complicated process of climbing dislocations and the permanent creation/annihilation of new nuclei on a small scale is not resolved. Instead, recovery and creation/annihilation of small nuclei are modeled by a stochastic Kolmogorov-Johnson-Mehl-Avrami equation [6,22,23],

$$\kappa_x^r(t) = \kappa^r(x, t) = e^{k(t-t_x)} - 1, \quad x \in \Omega. \quad (11)$$

This is a family of ordinary differential equations parameterized by  $x \in \Omega$  with  $\kappa_x^r(t) = \kappa^r(x, t)$  representing the density of the recovered material acting opposite to hardening. For  $t \approx t_x$ , the increase of  $\kappa^r$  is approximately linear. The exponent  $k \geq 0$ , possibly depending on  $x$ ,  $\alpha^0$ , and  $T$ , is a statistical growth rate. The array  $\{t_x\}_{x \in \Omega} \subset \mathbb{R}$  stores the start time (or age) of the nuclei, set constant in each grain and initialized to a random value near 0 at the beginning of the simulation. By definition,  $\kappa^r(x, t_x) = 0$ .

Let  $\kappa_{\text{crit}} > 0$  be the critical dislocation density. If  $(-\kappa)(\bar{x}, \bar{t}) > \kappa_{\text{crit}}$  for some  $\bar{x} \in \Omega$ ,  $\bar{t} > 0$ , around  $\bar{x}$  a new spherical grain  $\mathcal{G}$  is generated with critical radius  $r_{\text{crit}}$ . At this point, the new nucleus has overcome the energy barrier and is energetically favorable. In the new grain  $\mathcal{G}$ , it is set

$$\begin{aligned} \kappa(x, \bar{t}) : \\ &= \kappa^r(x, \bar{t}) \\ &: \\ &= 0, t_x \\ &: \\ &= \bar{t}, \alpha^0(x, \bar{t}) \\ &: \\ &= \alpha^0(\bar{x}) \quad \text{for all } x \\ &\in \mathcal{G}. \end{aligned} \quad (12)$$

Hence, the orientation of  $\mathcal{G}$  is constant and inherited from  $\alpha^0(\bar{x})$ , the rotation at the nucleation center. By setting  $t_{\bar{x}} := \bar{t}$ , the start time of the grain is reset and  $\mathcal{G}$  has no faster growth rate than initially for  $t=0$ .

For the rate  $k \geq 0$  in Eqn. (11), the ansatz

$$k = k(\alpha^0, x) := T \left| \nabla \alpha^0(x) \right|_2^2 := T \sum_{i=1}^3 \left| \nabla \alpha_i^0(x) \right|^2 \quad (13)$$

is made, with  $\nabla \alpha_i^0$  the weak gradient of the Sobolev function  $\alpha_i^0 \in H^1(\Omega)$ . Eqn. (13) is motivated by the experimental observation that the recovery rate is largest at the high-angle grain boundaries (where  $|\nabla \alpha^0|$  is large) and increases as  $T$  is increased. In most cases, a new recrystallized grain will continue to grow at the expense of its neighbors, since the jump of the dislocation density across the grain boundary, and hence  $V(\kappa)$ , is large, see Eqn. (16) below.

The recovery parameter  $\kappa^r \in \mathbb{R}$  enters in the computation of  $\kappa$  as

$$\kappa(\gamma, \kappa^r; \alpha^0, \kappa^0) := \left( \kappa^0 - \sum_{a=1}^{I_p} \left| \gamma_a - \gamma_a^0 \right| + \left( 1 - e^{-hk(\cdot, \alpha^0)} \right) (\kappa^r + 1) \right)_-.$$

In (14),  $|\gamma_a - \gamma_a^0|$  accounts for hardening due to plastic slip along the  $a$ -th slip system. In contrast,  $(1 - e^{-hk})(\kappa^r + 1)$  accounts for softening.

Eqn. (14) is derived from the constraint

$$hd_t^h F_p + hd_t^h (\kappa - \kappa^r) \leq 0 \quad (15)$$

which is a consequence of the Karish-Kuhn-Tucker conditions and which has to be satisfied with equality since the plastic flow occurs at the boundary of the set of feasible deformations, see, e.g. Refs. [11,8]. Due to Eqn. (11),

$$\begin{aligned} hd_t^h \kappa^r &= \kappa^r(t+h) - \kappa^r(t) = e^{k(t+h-t_x)} - e^{k(t-t_x)} \\ &= (1 - e^{-hk}) e^{k(t+h-t_x)} \\ &= (1 - e^{-hk}) (\kappa^r + 1). \end{aligned}$$

As  $hd_t^h F_p = \sum_{a=1}^{I_p} |\gamma_a - \gamma_a^0|$  and  $hd_t^h \kappa = \kappa - \kappa^0$ , this yields Eqn. (14). The negative part  $(z)_- := \min\{z, 0\}$  in (14) reflects that recovery can never exceed hardening and ensures  $(-\kappa) \geq 0$  for all  $t \geq 0$ . In the absence of softening, e.g. if  $k=0$ , it holds  $\kappa = \kappa^0 - \sum_a |\gamma_a - \gamma_a^0|$ , in particular  $\kappa \leq \kappa^0$ , and  $\kappa$  is monotonically decreasing.

#### 2.4. Movement of the grain boundaries

The movement of a grain wall is prescribed by the level set equation

$$\partial_t \omega + m \{ [V(\kappa)] + \text{div}_T(\xi) \} |\nabla \omega| = 0 \quad \text{in } \Omega, \quad (16)$$

controlling the growth in normal direction. Eqn. (16) does not include damping (thus no term  $\partial_n \omega$ ) and is formulated as the evolution of level sets to determine the positions of the moving grain boundaries. This level set approach is very flexible to topological changes. The values of  $\omega(t=0)$  are determined by the Ambrosio-Tortorelli approach, Eqn. (3), with the corresponding jump set

$$D := \cup_{i=1}^3 \text{supp}(\nabla v_i). \quad (17)$$

In (16),  $V(\kappa)$  denotes the jump of  $V(\kappa)$  along the interface,  $\text{div}_T := \nabla - \bar{n} \partial_n$  is the surface diffusion,  $\xi$  the Hoffmann-Cahn vector, see Refs. [20,42]. By  $\text{div}_T(\xi)$  diffusion of the wall due to curvature is represented;  $m = m(\alpha) \geq 0$  denotes the mobility of the domain wall. Experimental observations [16], [18], suggest the relationship  $v_n = mp$  for the velocity  $v_n$  in normal direction and the net pressure

$p=V(\kappa)+\text{div}_\Gamma(\xi)$  on the boundary. This leads to (16). Experiments have demonstrated further that the grain boundary mobility  $m$  depends on both temperature and grain misorientation. The exact dependence may be quite complicated. Even though systematic investigations seem to be missing, as a general guide line,  $m \approx 0$  for small angle boundaries (angles less than  $5^\circ$ ), whereas for large misorientations, an individual grain may grow rapidly, see [18], Section 5.2.21, and references therein. These considerations motivate  $m(\alpha) \sim R(\alpha)$ . In this article, the ansatz

$$m(\alpha) := |\nabla \alpha|_2 \quad (18)$$

is made for the numerical simulations.

### 2.5. The complete algorithm

This section ends with a summary of the complete algorithm for DRX.

0.\* **Initialization.** Given the noisy experimental data  $g$ , compute with (3) the smoothed orientations  $\alpha^0 = (\alpha_1^0, \alpha_2^0, \alpha_3^0)$  and the jump set  $D$ . Set

$$\kappa^0(x) := \begin{cases} -\frac{1}{2}\kappa_{\text{crit}} & \text{for } x \in D, \\ 0 & \text{for } x \in \Omega \setminus D. \end{cases} \quad (19)$$

Initialize  $\{t_x\}_{x \in \Omega}$  with random values close to 0.

1. **Plasticity/Hardening.** Compute  $(\varphi, \gamma, \alpha, \kappa)$  in  $\bar{\Omega}$  by solving (7) for given  $(\gamma^0, \alpha^0, \kappa^0)$  and given Dirichlet boundary data  $\varphi_D$  representing an uniaxial compression experiment,

$$\varphi_D(x, y, z, t) := (x, y, (1 - \beta t) z)^t \quad (20)$$

for a real constant  $0 < \beta < 1$ .

2. **Grain partitioning.** For  $\alpha = \alpha(t+h)$  computed in Step 1, apply the grain partitioning algorithm to determine the current grain structure.

3. **Recovery/Softening.** Compute  $\kappa^t$  by solving the Avrami equation (11). Introduce new spherical recrystallized grains of critical radius  $r_{\text{crit}}$  free of dislocations at  $\bar{x} \in \Omega$  provided  $(-\kappa(\bar{x})) > \kappa_{\text{crit}}$ .

4. **Propagation of the grain boundaries.** Move the grain walls from time  $t$  to time  $t+h$  due to (16) with the front tracking algorithm. Update  $\alpha$  accordingly.

5. **Loop.** Set  $\gamma^0 := \gamma$ ,  $\alpha^0 := \alpha$ ,  $\kappa^0 := \kappa(\gamma, \kappa^t)$ ,  $t := t+h$ . GOTO Step 1.

## 3. Numerical aspects

### 3.1. Plasticity and hardening

The computation of the plasticity and hardening part consists in solving the time-incremental minimization problem (7). This is done with the limited-memory Broyden-Fletcher-Goldfarb (L-BFGS) algorithm and finite differences developed in [10].

### 3.2. Front tracking algorithm

The front propagation is computed with a modified version of the algorithm in [36]. According to Eqn. (16), the normal velocity of an

interface  $\Gamma_{ij}$  between grains  $i$  and  $j$  satisfies

$$v_n = k_{ij} + e_i - e_j,$$

where  $k_{ij}$  denotes the mean curvature of  $\Gamma_{ij}$ , and  $e_i - e_j$  are bulk energy differences,

$$e_i - e_j = m(\alpha) [V(\kappa)].$$

As before,  $V(\kappa)$  denotes the jump of  $V(\kappa)$  across  $\Gamma_{ij}$ .

Let  $\eta > 0$  be a small time step such that  $h = N\eta$  for some  $N \in \mathbb{N}$ , where  $h > 0$  is the fixed time step of the Cosserat minimization (7).

Front tracking algorithm (Propagate the fronts from time  $t$  to time  $t+h$ ).

1 Initialization: Let  $r \geq 2$  grains be present initially. FOR  $i=1, \dots, r$ : Set  $\omega_i(x, t)$  as the characteristic function of the  $i$ -th grain. Set  $j:=1$ .

$$\begin{aligned} 2 \quad \omega^j(x, 0) &: \\ &= \omega(x, t + (j-1)\eta) \\ \text{DiffusionSet} &: \\ &= (\omega_i(x, t + (j-1)\eta))_{1 \leq i \leq r} \end{aligned}$$

For  $i=1, \dots, r$ : Compute  $\omega_i^j(x, \eta)$  by solving the first time step of the diffusion problem

$$\begin{aligned} \partial_t \omega_i^j &= \Delta \omega_i^j \quad \text{in } \Omega, \\ \partial_n \omega_i^j &= 0 \quad \text{at } \partial\Omega. \end{aligned} \quad (21)$$

3 Sharpening: For each  $x \in \Omega$

Let  $\hat{\omega}^j := (\omega_l^j, \omega_m^j, \omega_n^j)(x, \eta)$ , where  $\omega_l^j(x, \eta)$ ,  $\omega_m^j(x, \eta)$ ,  $\omega_n^j(x, \eta)$  are the three largest values of  $(\omega_i^j(x, \eta))_{1 \leq i \leq r}$ . Set

$$(\omega_l, \omega_m, \omega_n)(x, t + j\eta) := \begin{cases} (1, 0, 0), & \text{if } \pi(\hat{\omega}^j) \in R_1, \\ (0, 1, 0), & \text{if } \pi(\hat{\omega}^j) \in R_2, \\ (0, 0, 1), & \text{if } \pi(\hat{\omega}^j) \in R_3. \end{cases} \quad (22)$$

Set  $\omega_i(x, t+j\eta) := 0$  for all  $i \in \{1, \dots, r\} \setminus \{l, m, n\}$ .

4 Loop: Set  $j:=j+1$ . WHILE  $j < N+1$  GOTO Step 2

The regions  $R_1, R_2, R_3$  introduced in Eqn. (22) are displayed in Fig.

1. The transition points  $p_{ij}$  are defined in (23).

For any time  $s \geq 0$ , the moving grain boundaries are determined by

$$\partial \{x \in \Omega \mid \omega_i(x, s) = 1\}.$$

In Eqn. (22),  $\pi: [0, 1]^3 \rightarrow \Sigma$  denotes the projection of  $\hat{\omega}^j$  to barycentric coordinates of the projection triangle, i.e.

$$\pi(\omega_1, \omega_2, \omega_3) := \frac{1}{\omega_1 + \omega_2 + \omega_3} (\omega_1, \omega_2, \omega_3).$$

The projector  $\pi$  replaces the transfer function  $f$  in [36] for general diffusion problems which is required when the diffusion constants in (21) differ. Eqn. (22) states that by the projection triangle algorithm,

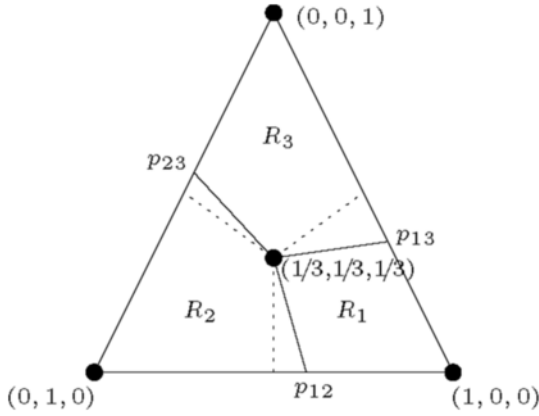


Fig. 1. Projection triangle  $\Sigma$  with (solid) and without (dotted) bulk components  $e_j$ .

every  $\omega \in R_i$  is mapped to the corner of  $R_i$  (i.e. to  $(0,0,1)$ ,  $(1,0,0)$  or  $(0,1,0)$ ).

The transition points  $p_{ij} \in \mathbb{R}^3$  are defined by

$$\begin{aligned} p_{12} &= \left( \frac{1}{2} + \frac{1}{2} (e_1 - e_2) \sqrt{\frac{\eta}{2\pi}}, \frac{1}{2} - \frac{1}{2} (e_1 - e_2) \sqrt{\frac{\eta}{2\pi}}, 0 \right), \\ p_{13} &= \left( \frac{1}{2} - \frac{1}{2} (e_3 - e_1) \sqrt{\frac{\eta}{2\pi}}, 0, \frac{1}{2} + \frac{1}{2} (e_3 - e_1) \sqrt{\frac{\eta}{2\pi}} \right), \\ p_{23} &= \left( 0, \frac{1}{2} + \frac{1}{2} (e_2 - e_3) \sqrt{\frac{\eta}{2\pi}}, \frac{1}{2} - \frac{1}{2} (e_2 - e_3) \sqrt{\frac{\eta}{2\pi}} \right). \end{aligned} \quad (23)$$

These definitions induce a CFL-condition:  $\eta > 0$  must be small enough (or  $N \in \mathbb{N}$  in  $h = N\eta$  must be large enough) to ensure  $p_{ij} \in \Sigma$ .

In the presence of multiple grains, the level set approach may lead to topological errors, i.e. voids may form or neighboring level sets may overlap. To avoid this, as explained in [29], in regular intervals, a correction step is necessary. Every 10th step, the level sets are redefined by setting

$$\omega_i := \frac{1}{2} \left[ \omega_i - \max_{\substack{1 \leq j \leq r \\ j \neq i}} \omega_j \right] \quad \text{in } \Omega, \quad i = 1, \dots, r.$$

The parabolic problem (21) is discretized in time with the implicit Euler scheme

$$(\text{Id} + \eta S) \omega^{j+1} = \omega^j, \quad (24)$$

where the stiffness matrix  $S$  is a block matrix originating from the spatial discretization of  $-\Delta$  with free boundary conditions in  $\mathbb{R}^3$ . The discrete system (24) is solved with a (preconditioned) conjugate-gradient method.

#### 4. Simulations

In the simulations, a 3D specimen is deformed plastically according to Eqn. (20). Of interest are the resulting grain distribution and the mechanical properties of the polycrystal. All computations are dimensionless since for finite-strain Cosserat media it is usually impossible to identify the correct Cosserat parameters corresponding to experimental data, see Refs. [30,24].

Unless stated otherwise, the simulations share the parameters

$$\begin{aligned} t \in [0, 1], \quad \beta = 0.1, \quad h = 0.001, \quad \varepsilon = 10^{-4}, \quad M_{\text{ext}} = 0, \quad f_{\text{ext}} = \mu_c = 0, \\ \lambda = \mu = 0.025, \quad \mu_2 = 0.002, \quad \rho = 0.2, \quad \sigma_Y = 1.0; \quad r_c = 0.04; \quad \kappa_{\text{crit}} = 0.2, \\ \sigma = 0.4; \quad \tau = 5.0; \quad \delta_{\text{TOL}} = 0.005. \end{aligned}$$

Here,  $\varepsilon$  is the regularization parameter of  $|\cdot|$ , see Eqn. (14) in Ref. [10].

Five different initial grain distributions have been used in the simulations, obtained from experimental measurements with varying spatial resolutions. Table 1 Gives an overview and shows the corresponding numerical costs for the solution of one time step of (7).

Fig. 2 renders exemplary one grain distribution obtained from measurements for the iron-nickel-chromium austenitic alloy 800H. The slip systems for this material are taken from [41]. Fig. 3 shows exemplary two cross-sections of the computed grain structure starting from distribution ‘‘G4’’.

The first important result of the simulations concerns the long-time behavior of the grain distribution, as outlined in Fig. 4.

As can be seen, basically two different states occur. The first state, at the beginning of the simulations, is characterized by the absence of newly recrystallized grains. The grain structure steadily

Table 1

Comparison of different initial grain structures. ‘‘time’’ lists the computation time for the solution of the first time step of (7) with the L-BFGS algorithm (single desktop PC; Intel Dual-Core E7400 (2.8 GHz) and 4 GB RAM).

Name	Reference domain	Resolution	Grains	Nodes	Unknowns	Time
G1	$\Omega = (0,1)^3$	$16 \times 16 \times 7$	62	1792	10180	2.5 s
G2	$\Omega = (0,1)^2 \times (0,2)$	$16 \times 16 \times 16$	92	4096	24616	13.4 s
G3	$\Omega = (0,2)^2 \times (0,1)$	$32 \times 32 \times 7$	121	7168	42172	34.2 s
G4	$\Omega = (0,2)^3$	$32 \times 32 \times 15$	183	15360	96540	121 s
G5	$\Omega = (0,2)^2 \times (0,4)$	$32 \times 32 \times 32$	328	32768	212072	319 s

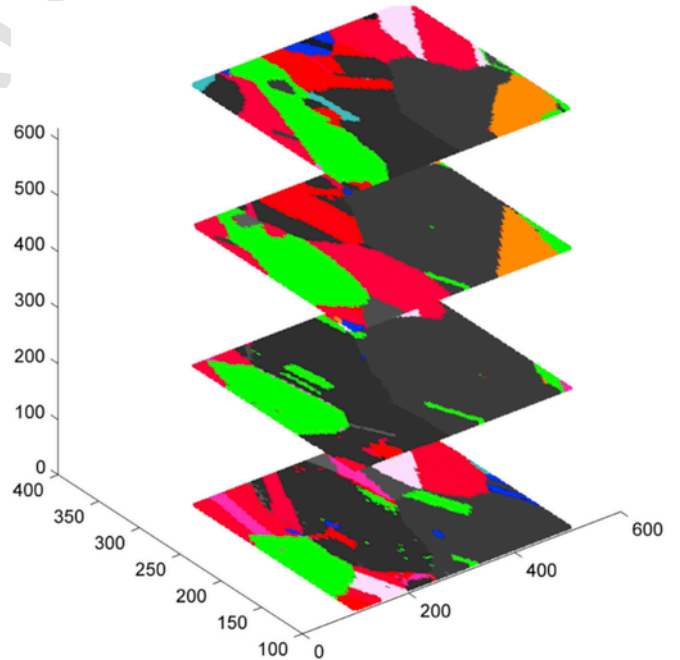


Fig. 2. Four cross sections of the initial grain distribution ‘‘G1’’ computed from experimental data of the alloy 800H with 62 grains and resolution  $16 \times 16 \times 7$ .

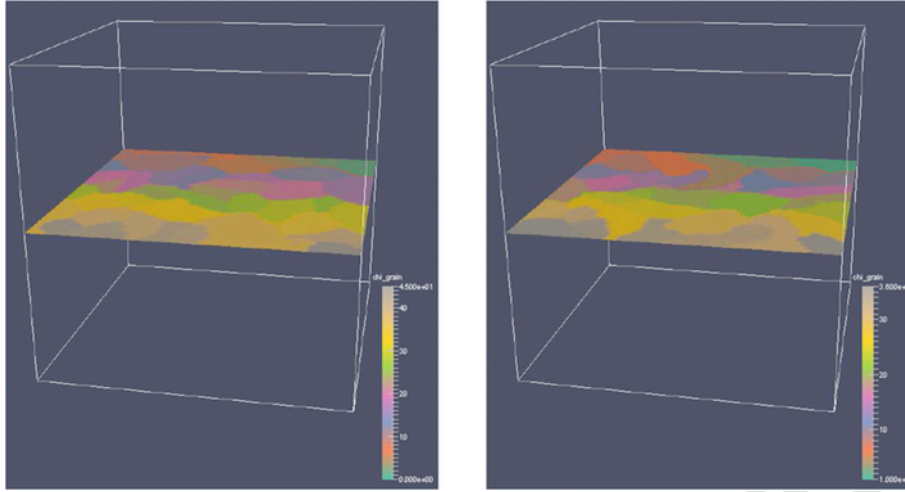


Fig. 3. Cross-section of the computed grain structure at  $z=0.5$  for the initial distribution "G4" and  $t=0.45$  (left),  $t=0.95$  (right).

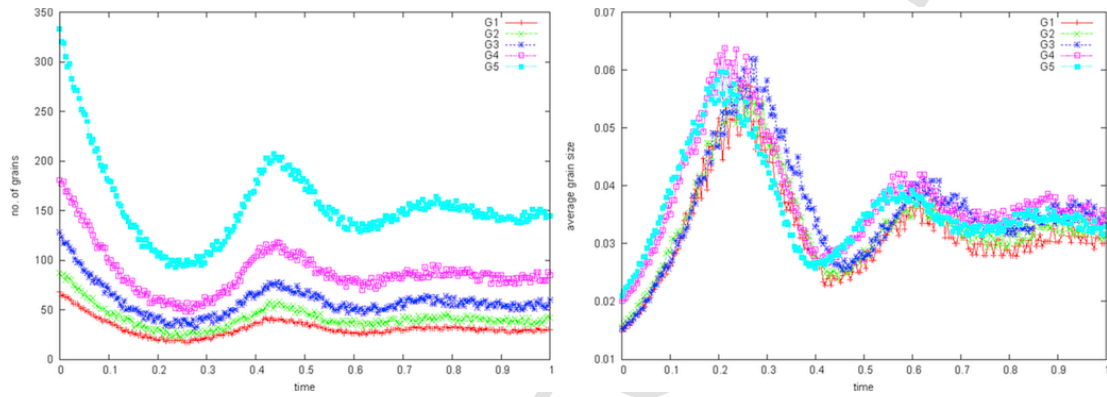


Fig. 4. Long-time behavior of the simulated grain distribution for lattice geometries G1-G5 of Table 1. Left: Number of grains. Right: Average grain size  $D$ .

coarsens and there is one distinct configuration where the total number of grains is minimal (and the average size  $D$  is maximal). In the transition from the first to the second state, recrystallization kicks in. New recrystallized grains of smaller size are formed and  $D$  decreases. This second state is characterized by oscillations which become smaller and smaller until remarkably, up to small deviations,  $D$  is constant.

The two different states also manifest themselves in the computed flow curves, Fig. 5. An initial hardening period is followed by a period with smaller and smaller oscillations that tend toward a steady state. The computations also demonstrate that  $\sigma$  decreases when  $T$  is increased.

Fig. 4 suggests that the equilibrium average grain size  $D$  in the third state is a universal quantity, possibly depending only on global parameters kept fixed during the simulations. These considerations motivate to study the law

$$\sigma_Y \sim D^p \quad (26)$$

between the yield stress  $\sigma_Y$  and the average grain size  $D$ , where  $p$  is a suitable exponent. For  $p = -\frac{1}{2}$ , Eqn. (26) relates to the famous Hall-Petch relation.

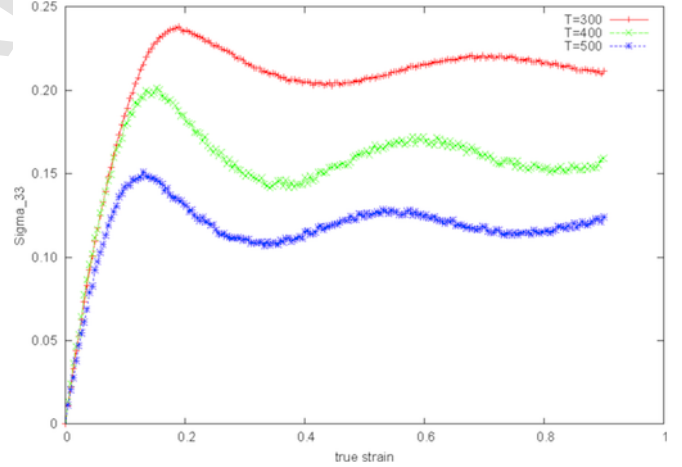


Fig. 5. Computed component  $\sigma_{33}$  of the 1. Piola Kirchhoff stress  $\sigma = \frac{\partial W_{st}(U_e)}{\partial F}$  for different temperatures and geometry G5.

In order to study (26), for  $N \geq 2$  simulations and input values  $\{\sigma_{Y,n}\}_{1 \leq n \leq N}$  (all other parameters are unchanged), the average grain

sizes  $\{D_n\}_{1 \leq n \leq N}$  for large  $t$  are computed numerically. The exponent  $p$  is computed by the formula

$$p = \frac{\ln(\sigma_{Y,n}/\sigma_{Y,n+1})}{\ln(D_n/D_{n+1})} = \frac{\ln(\sigma_{Y,n}) - \ln(\sigma_{Y,n+1})}{\ln(D_n) - \ln(D_{n+1})}. \quad (27)$$

Fig. 6 has the details. As can be seen, the simulations predict an exponential dependence of  $p$  on  $\sigma_Y$  (with certain changes depending on the chosen geometry). However,  $p$  also depends on the parameter  $\delta_{TOL}$  from Eqn. (4), since this parameter is crucial for the number of grains identified by the algorithm.

## 5. Discussion

In this article, a new model for dynamic recrystallization is proposed. It combines the Ambrosio-Tortorelli functional from image analysis with the Cosserat theory of crystal plasticity to derive an algorithm that automatically identifies the grain structure of the polycrystal. The micro-rotations of the Cosserat model determine the orientations and wall mobilities of the new recrystallized grains. The model is completed with an Avrami equation to model softening and a level set method to propagate the grain walls.

The simulations demonstrate that after a first initialization period where the initial grain structure changes and the material hardens, there is a second oscillatory period with smaller and smaller fluctuations tending for large  $t$  toward a stable equilibrium with an (almost) constant average grain size  $D$ .

The proposed method differs significantly from the approach in [15] where homogenization techniques are applied to a periodic grain structure with fixed connectivity to simulate the small-strain kinematics of elasto-plastic Cosserat crystals. In this article, the partitioning

into (sub-) grains is achieved directly from the local deformations and rotation fields of the Cosserat equations, allowing the grain topology and the connectivity of the grains to be non-periodic and to change with time.

At present, the proposed method still has some severe shortcomings. Firstly, the spatial resolution of the experimental grain data in  $z$ -direction is low, affecting the precision of the simulations. Secondly, the simulations are non-dimensional and depend on finite size effects. The choice of the parameters  $\delta_{TOL}$  in Eqn. (4),  $\sigma$ ,  $\tau$ ,  $\delta$  in Eqn. (3), the critical radius  $r_{crit}$ , the growth rate of the newly recrystallized grains, the Cosserat parameter  $\mu_2$ , and the softening law all influence the computations. Clearly, the computed exponent  $p$  depends on  $\delta_{TOL}$ , as Fig. 6 indicates. The oscillatory second part in the curves of Fig. 5 depends in a complicated way on the total dislocation density and the number/geometry of the grains present (hence also on  $\delta_{TOL}$ ). For a more complete understanding of DRX, it would be very desirable to understand in detail the complicated mechanisms involved here.

Alternative to the Ambrosio-Tortorelli approach, several other methods have been developed that can potentially be used in an automatic grain identification process. One may resort to algebraic topology [4], or apply mesh-free Hamiltonian functionals in the spirit of [25]. Another possibility is stochastic methods, e.g. stochastic homogenization, [39].

## Uncited references

[38]; [40]

## Acknowledgments

TB wishes to thank Prof. G. Gottstein and Prof. S. Luckhaus for valuable discussions.

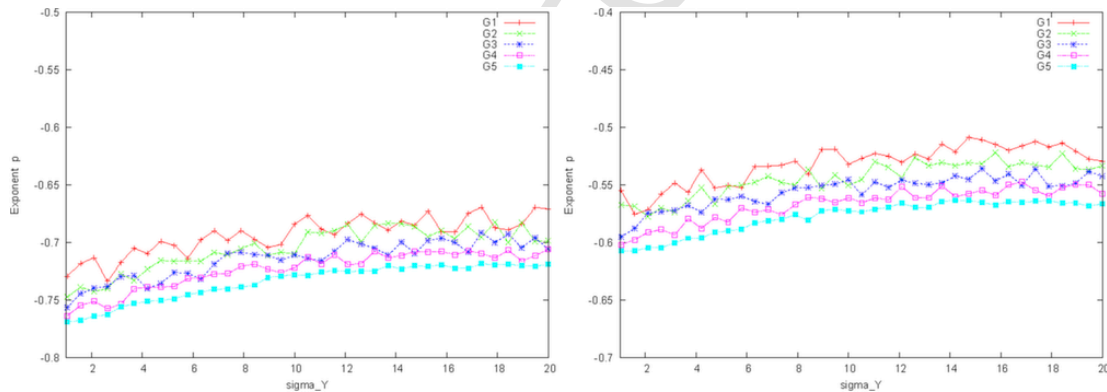


Fig. 6. Growth exponent  $p$  as a function of  $\sigma_Y$  for the 5 different lattice geometries of Table 1. Left:  $\delta_{TOL}=0.005$ . Right:  $\delta_{TOL}=0.002$ .

## References

- [1] G. Abrivard, E.P. Busso, S. Forest, B. Appolaire, Phase field modelling of grain boundary motion driven by curvature and stored energy gradients. Part I: theory and numerical implementation, *Phil Mag* 92 (2012) 3618–3642.
- [2] G. Abrivard, E.P. Busso, S. Forest, B. Appolaire, Phase field modelling of grain boundary motion driven by curvature and stored energy gradients. Part II: application to recrystallisation, *Phil Mag* 92 (2012) 3643–3664.
- [3] A. Acharya, J. Bassani, Lattice incompatibility and a gradient theory of crystal plasticity, *J Mech Phys Solids* 48 (2000) 2213–2230.
- [4] M.P. Ariza, M. Ortiz, Discrete crystal elasticity and discrete dislocations in crystals, *Arch Rat Mech Anal* 178 (2005) 149–226.
- [5] L. Ambrosio, V.M. Tortorelli, Approximation of functionals depending on jumps by elliptic functionals  $\Gamma$ via convergence, *Comm Pure Appl Math* 43 (1990) 999–1036.
- [6] M. Avrami, Kinetics of phase change. III: granulation, phase change and microstructure, *J Chem Phys* 9 (1941) 177–184.
- [7] T. Blesgen, S. Luckhaus, The dynamics of transition layers in solids with discontinuous chemical potentials, *Math Meth Appl Sci* 29 (2006) 525–536.
- [8] T. Blesgen, Deformation patterning in Cosserat plasticity, *Model Simul Mater Sci Eng* 21 (3) (2013) 35001–35012.
- [9] T. Blesgen, Deformation patterning in three-dimensional large-strain Cosserat plasticity, *Mech Res Comm* 62 (2014) 37–43.
- [10] T. Blesgen, On rotation deformation zones for finite-strain Cosserat plasticity, *Acta Mech* 226 (2015) 2421–2434.
- [11] C. Carstensen, K. Hackl, A. Mielke, Non-convex potentials and microstructures in finite-strain plasticity, *Proc Roy Soc A* 458 (2002) 299–317.
- [12] M. Crumbach, M. Goerdeler, G. Gottstein, Modelling of recrystallisation textures in aluminium alloys: I. Model set-up and integration, *Acta Mater* 54 (2006) 3275–3289.
- [13] B. Derby, M. Ashby, On dynamic recrystallization, *Scr Met* 21 (1987) 879–884.
- [14] I. Fonseca, G.A. Francfort, Relaxation in BV versus quasiconvexification in  $W^{1,p}$ : a model for the interaction between fracture and damage, *Calc Var* 3 (4) (1995) 407–446.
- [15] S. Forest, F. Barbe, G. Cailletaud, Cosserat modelling of size effects in the mechanical behaviour of polycrystals and multi-phase materials, *Int J Solids Struct* 37 (2000) 7105–7126.
- [16] M. Frommert, G. Gottstein, Mechanical behaviour and microstructure evolution during steady-state dynamic recrystallization in the austenitic steel 800H, *Mater Sci Eng A* 506 (2008) 101–110.
- [17] H. Hallberg, A modified level set approach to 2D modeling of dynamic recrystallization, *Model Sim Mat Sci Eng* 21 (2013) 1–33.
- [18] F.J. Humphreys, M. Hatherly, *Recrystallization and related annealing phenomena*, second ed., Pergamon publishing, New York, 2004.
- [19] E.W. Hart, A phenomenological theory for plastic deformation of polycrystalline metals, *Acta Met* 18 (1970) 599–610.
- [20] D.W. Hoffmann, D.W., J.W. Cahn, A vector thermodynamics for anisotropic surfaces-I. Fundamentals and applications to plane surface junctions, *Surf Sci* 31 (1972) 368–388.
- [21] M.F. Ibrahim, H.R. Ammar, A.M. Samuel, M.S. Soliman, F.H. Samuel, On the impact toughness of Al-15 vol.% B4C metal matrix composites, *Compos Part B Eng* 79 (2015) 83–94.
- [22] W.A. Johnson, R.F. Mehl, Reaction kinetics in processes of nucleation and growth, *Rans Am Inst Min Met Eng* 135 (1939) 416–458.
- [23] A.N. Kolmogorov, Statistical theory of crystallization of metals. (in russian), *Izv Akad Nauk SSSR, Ser Mat* 1 (1937) 355–359.
- [24] R.S. Lakes, On the torsional properties of single osteons, *J Biomech* 25 (1995) 1409–1410.
- [25] S. Luckhaus, L. Mugnai, On a mesoscopic many-body Hamiltonian describing elastic shears and dislocations, *Cont Mech Thermodyn* 22 (2010) 251–290.
- [26] M. Luton, M. Sellars, Dynamic recrystallization in nickel and nickel-iron alloys during high temperature deformation, *Acta Met* 17 (1969) 1033–1043.
- [27] V. Mantič, *Mathematical methods and models in composites*, World Scientific Press, 2013.
- [28] H. Mecking, U.F. Kocks, Kinetics of flow and strain-hardening, *Acta Met* 29 (1981) 1865–1875.
- [29] B. Merriman, J.K. Bence, S.J. Osher, Motion of multiple junctions: a level set approach, *J Comp Phys* 112 (1994) 334–363.
- [30] P. Neff, A finite-strain elastic-plastic Cosserat theory for polycrystals with grain rotations, *Int J Eng Sci* 44 (2006) 574–594.
- [31] M. Ortiz, E. Repetto, Nonconvex energy minimization and dislocation structures in ductile single crystals, *J Mech Phys Solids* 47 (2) (1999) 397–462.
- [32] E.I. Poliaki, J.J. Jonas, A one-parameter approach to determining the critical conditions for the initiation of dynamic recrystallization, *Acta Mater* 44 (1996) 127–136.
- [33] M. Quaresimin, P.A. Carraro, L.P. Mikkelsen, N. Lucato, L. Vivian, P. Brondsted, et al., Damage evolution under cyclic multiaxial stress state: a comparative analysis, between glass/epoxy laminates and tubes, *Comp B Eng* 61 (2014) 282–290.
- [34] W. Roberts, B. Ahlblom, A nucleation criterion for dynamic recrystallization during hot working, *Acta Met* 26 (1978) 801–813.
- [35] A.D. Rollett, Overview of modeling and simulation of recrystallization, *Prog Mater Sci* 42 (1997) 79–99.
- [36] S.J. Ruuth, A diffusion-generated approach to multiphase motion, *J Comp Phys* 145 (1998) 166–192.
- [37] T. Sakai, J.J. Jonas, Dynamic recrystallization: mechanical and microstructural considerations, *Acta Met* 32 (1984) 189–209.
- [38] R. Sandström, R. Lagneborg, A model for hot working occurring by recrystallization, *Acta Met* 23 (1975) 387–398.
- [39] I.G. Stratis, A.N. Yannacopoulos, Homogenisation theory for deterministic and random bianisotropic media, *Comp B* 43 (2012) 2513–2520.
- [40] H.P. Stüwe, B. Ortner, Recrystallization in hot working and creep, *Metal Sci* 8 (1974) 161–167.
- [41] Vasudevan, V., Sham, S., Carroll, L. report Mechanisms governing the creep behavior of high temperature alloys for generation iv nuclear energy systems. Report 09–776 to U.S. Dept. Of energy, Univ. of Cincinnati.
- [42] A.A. Wheeler, Cahn-Hoffmann  $\xi$ -vector and its relation to diffuse interface models of phase transitions, *J Stat Phys* 95 (1999) 1245–1280.
- [43] G.M. Zhao, Y.Q. Yang, W. Zhang, X. Luo, B. Huang, Y. Chen, Microstructure and grain growth of the matrix of SiCf/Ti6Al4V composites prepared by the consolidation of matrix-coated fibers in the  $\beta$  phase field, *Compos B Eng* 52 (2013) 155–163.
- [44] T.I. Zohdi, P. Wriggers, *An introduction to computational micromechanics*, Springer, Berlin, 2008.